Cell PRESS
Structure
Article

The Deletion of Exon 3 in the Cardiac Ryanodine Receptor Is Rescued by β Strand Switching

Paolo A. Lobo,[1] Lynn Kimlicka,[1] Ching-Chieh Tung,[1] and Filip Van Petegem[1,*]
[1]Department of Biochemistry and Molecular Biology, University of British Columbia, 2350 Health Sciences Mall, room 2.320, Vancouver, BC V6T 1Z3, Canada
*Correspondence: filip.vanpetegem@gmail.com
DOI 10.1016/j.str.2011.03.016

SUMMARY

Mutations in the cardiac Ryanodine Receptor (RYR2) are linked to triggered arrhythmias. Removal of exon 3 results in a severe form of catecholaminergic polymorphic ventricular tachycardia (CPVT). This exon encodes secondary structure elements that are crucial for folding of the N-terminal domain (NTD), raising the question of why the deletion is neither lethal nor confers a loss of function. We determined the 2.3 Å crystal structure of the NTD lacking exon 3. The removal causes a structural rescue whereby a flexible loop inserts itself into the β trefoil domain and increases thermal stability. The exon 3 deletion is not tolerated in the corresponding RYR1 domain. The rescue shows a novel mechanism by which RYR2 channels can adjust their Ca^{2+} release properties through altering the structure of the NTD. Despite the rescue, the deletion affects interfaces with other RYR2 domains. We propose that relative movement of the NTD is allosterically coupled to the pore region.

INTRODUCTION

Excitation-contraction (E-C) coupling in cardiac and skeletal muscle requires the rapid release of Ca^{2+} from the sarcoplasmic reticulum (SR) into the cytoplasm. This release is mediated by ryanodine receptors (RyRs), ~2.2 MDa channels located in the SR membrane. Three different mammalian isoforms have been isolated to date (RYR1-3). Whereas RYR1 predominates in skeletal muscle, RYR2 is the major type found in cardiac myocytes (Giannini et al., 1995). RyR3 is more ubiquitous and was originally found in rabbit brain (Hakamata et al., 1992). Electron microscopy studies have shown that the bulk of the RyR structure is located in the cytoplasm, with only 10% forming the transmembrane region (Liu et al., 2001; Ludtke et al., 2005; Samso et al., 2005, 2009; Sharma et al., 1998; Wang et al., 2007). Opening and closing of the channel is linked to long-range allosteric motions within the cytoplasmic "foot" (Samso et al., 2009). It forms docking sites for many auxiliary proteins that affect the gating properties of the channel (Bers, 2004; Lehnart et al., 2005; Marx et al., 2000; Zalk et al., 2007). A number of high-resolution studies have described the structures of individual RyR domains, including the N-terminal domains (Amador et al., 2009; Lobo and Van Petegem, 2009; Tung et al., 2010) and a binding site for the Ca^{2+} binding proteins calmodulin (Maximciuc et al., 2006) and S100A1 (Wright et al., 2008).

RYR1 and RYR2 are targets for an increasing list of disease mutations. Individual amino acid substitutions in RYR1 can result in malignant hyperthermia (MH) and central core disease (CCD)(Cabello and Ricoy-Campo, 2003; MacLennan and Phillips, 1992; Robinson et al., 2006; Shepherd et al., 2004). Substitutions in RYR2 have been found to underlie catecholaminergic polymorphic ventricular tachycardia (CPVT) and arrhythmogenic right ventricular dysplasia type 2 (ARVD2), conditions triggered in response to physical or emotional stress, resulting in cardiac arrhythmias and sometimes sudden cardiac death (George et al., 2007; Laitinen et al., 2001; Priori et al., 2001; Thomas et al., 2007). RyRs are activated by Ca^{2+} and most disease mutations characterized to date confer a gain of function to the channels: they have a lowered threshold for either cytoplasmic Ca^{2+} (calcium induced calcium release [CICR]) or SR Ca^{2+} levels (store overload induced calcium release [SOICR]) and are more sensitive to activating agents (George et al., 2003; Jiang et al., 2002, 2004, 2005, 2008; Koop et al., 2008; MacLennan and Chen, 2009). In the case of cardiac RyRs, the increase in cytosolic Ca^{2+} leads to an increased activity of the Na^{+}/Ca^{2+} exchanger, resulting in delayed after depolarizations (DADs) (Fozzard, 1992; Lehnart et al., 2008; Marban et al., 1986).

A large number of mutations cluster in the N-terminal ~600 residues of RYR2 (Medeiros-Domingo et al., 2009). A very severe form of CPVT is caused by removal of the entire third exon in RYR2 (Bhuiyan et al., 2007; Marjamaa et al., 2009; Medeiros-Domingo et al., 2009). In addition to the typical CPVT-related symptoms, patients with the RYR2 exon 3 deletion develop atrioventricular block, sinoatrial node dysfunction, atrial fibrillation, and atrial standstill (Bhuiyan et al., 2007).

The RYR2 exon 3 is situated in the N-terminal domain (residues 1–217, referred to as "RYR2A" throughout this text). A recent crystal structure of this domain shows a fold consisting of 12 β strands forming a β trefoil core (Lobo and Van Petegem, 2009). In addition, a 3_{10} helix and α helix are found before and after strand β_4, respectively. An almost identical fold is found in RYR1 (Amador et al., 2009; Lobo and Van Petegem, 2009; Tung et al., 2010). Exon 3 forms a crucial part of the structure, consisting of 35 amino acids that build up a loop region, the 3_{10} helix, β_4, and the α helix. Being intimately entangled with the remainder of the domain, removal of just the β strand would already be predicted to cause misfolding of RYR2A, something that would likely affect folding of multiple RyR domains and result

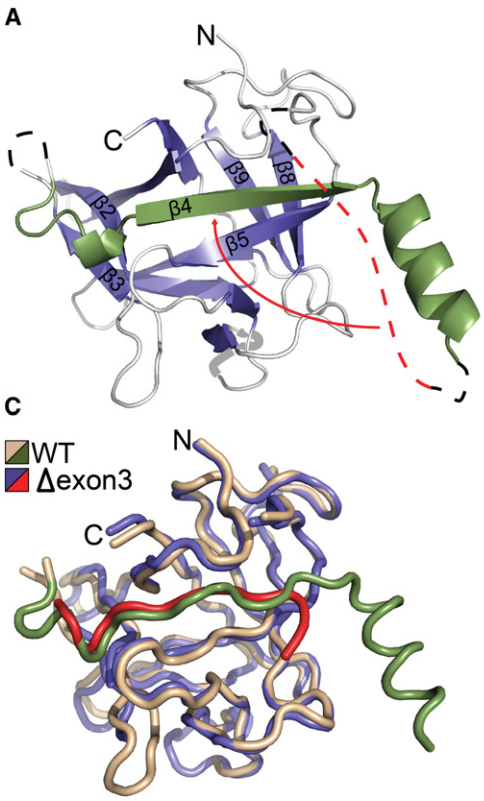

Figure 1. Overall Structure

(A) Cartoon representation of wild-type RyR2A. Exon 3 is shown in green, and the flexible loop, replacing exon 3 in the RYR2A Δexon3 structure, is indicated by a red dotted line.

(B) Cartoon representation of RYR2A Δexon3, shown in the same orientation. The rescue segment is shown in red. Electron density for the rescue segment in shown in Figure S1.

(C) Superposition of RYR2A and RYR2A Δexon3.

in an overall loss-of-function phenotype. Although severe, the exon 3 deletion is not strictly lethal, and its CPVT symptoms suggest mechanisms similar to individual RYR2 point mutations conferring a gain of function. How is such a drastic deletion tolerated in the ryanodine receptor, and why does it not cause loss of function? We previously found that RYR2A Δexon3 is still soluble and does not aggregate (Lobo and Van Petegem, 2009). Here, we reinvestigate the folding properties and show a 2.3 Å crystal structure of RYR2A Δexon3 (residues 1–217). The structure shows a drastic rearrangement that rescues the N-terminal domain. These motions underline an unusual structural plasticity of the RYR2 N-terminal region, and show that RyRs have adopted an extra strategy to fine-tune their functional properties.

RESULTS

Crystal Structure of the RYR2 Δexon3 N-Terminal Domain

The exon 3 deletion in RYR2 abolishes residues 57 to 91 in the N-terminal domain (RYR2A). It removes a β strand (β_4) that is part of a β trefoil core, and an α helix (Figure 1A). The deletion did not seem to cause unfolding or aggregation of the domain, but even seemed to increase the melting temperature (Lobo and Van Petegem, 2009). How is it possible that removal of a β strand from a β sheet enhances the thermal stability?

In order to investigate this paradox, we solved the crystal structure of the RYR2A Δexon3 domain at 2.3 Å. In par with the improved thermal stability, the protein was easier to crystallize than wild-type, resulting in over 50 initial crystallization hits in a random screen of 7x96 conditions, compared with only two hits for wild-type RYR2A.

We initially used phases from a model consisting of the RYR2A wild-type structure, missing all exon 3 residues. The RYR2A Δexon3 crystals contain two molecules in the asymmetric unit. All further comparisons, unless noted otherwise, are performed with chain B. Surprisingly, difference electron density was clearly present in the region previously encoded by exon 3. Although no density was visible for the α helix, another element compensated for the loss of both β_4 and the 3_{10} helix. The density was of sufficient quality to assign the right sequence to this region, and the identity of two methionines in the segment was confirmed by anomalous data collected on selenomethionine-substituted protein crystals (see Figure S1 available online). The complete structure of RYR2A Δexon3 is shown in Figure 1B. The protein is folded as a β trefoil, but evidently misses the α helix. Instead of forming a collapsed structure, the main chain atoms seem to superpose very well with the ones in wild-type RYR2A (Figure 1C). Both structures superpose with an rmsd of 0.901 Å for 136 C_α atoms (based on superposition of chain A in both models).

Identity of the New β Strand

The resolution of the structure, together with the anomalous signal, allowed an unambiguous assignment of the residues replacing β_4 and the 3_{10} helix. These correspond to the sequence ^{93}VDVEKWKFMMKT^{104}, which is part of a flexible loop connecting α_1 to β_5 in wild-type RYR2A. Both RYR1A and RYR2A have flexible linkers connecting α_1 and β_5, but it is particularly longer in RYR2, containing a 12 amino acid insertion that is unique to RYR2 (Lobo and Van Petegem, 2009). This represents an unprecedented case of "rescue" of a drastic disease mutation: an otherwise flexible loop becomes a β strand, and thus preserves the domain core.

Comparison of the β_4 Fit into the β Sheet

An alignment of the residues forming the fourth β strand in RYR2A and RYR2A Δexon3 shows that the identities of the corresponding residues are completely dissimilar (Figures S2 and S3). How is it possible that two entirely different sequences can fit into the same complementary surface? Figures 2A and 2B compare the β_4 region in RYR2A and RYR2A Δexon3. In both

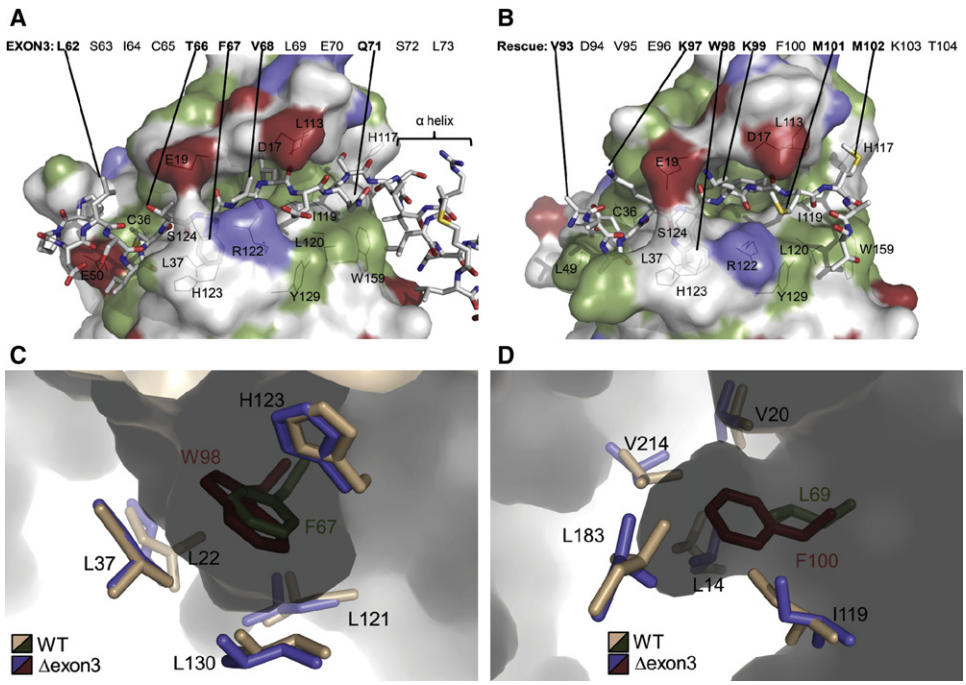

Figure 2. Contacts with Exon 3 and the Rescue Segment

(A and B) Comparison of contacts between exon 3 and the remainder of wild-type RYR2A (A) and between the rescue segment and the rest of the RYR2A Δexon3 domain (B). Exon 3 and the rescue segment are shown as sticks. The remainder is shown in surface representation, indicating hydrophobic (green), and positively (blue) and negatively (red) charged side chains.

(C) Inner view of the deep pocket binding F67 (RYR2A) or W98 (RYR2A Δexon3). Side chains lining the pocket are shown in sticks.

(D) Inner view of the deep pocket binding L69 (RYR2A) or F100 (RYR2A Δexon3). A superposition of exon 3 and the rescue segment is shown in Figure S3.

cases, the strand binds to a predominantly hydrophobic surface. The most extensive interactions are formed by two hydrophobic residues binding in deep pockets. In RYR2A, one pocket is filled by the side chain of F67, whereas the other is only partially filled by L69. In RYR2A Δexon3, these are replaced by W98 and F100, both of which provide more contacts with the hydrophobic residues in the pockets (Figures 2C and 2D). These extra contacts show that the rescue segment adopts a better fit into the remainder of the domain, likely causing the improved stability of RYR2A Δexon3.

Additional Structural Plasticity

In addition to the large rearrangement, structural plasticity is present in another β strand (β_3). The conformation between both chains in the asymmetric unit differs: in chain A, the conformation is very similar to the one observed in wild-type RYR2A, but in chain B there is a one amino acid shift in the sequence: a pocket normally filled up by L49 is now filled up by F48 (Figure 3A; Figure S4). The shift in register is accompanied by a shift in the main chain away from the center of the protein. This allows the bulkier phenylalanine side chain to fit in a pocket otherwise filled up by the leucine residue. This structural rearrangement is allowed, in part, by flexible loops: both linkers connecting β_3 to neighboring strands have missing electron density and are thus interpreted to be flexible. Because β_3 is part of a β sheet, its shift is correlated with a translation of the neighboring strand (β_2), which further induces changes in the 3_{10} helix (Figure 3B). The rearrangement of β_3 may be the direct result of

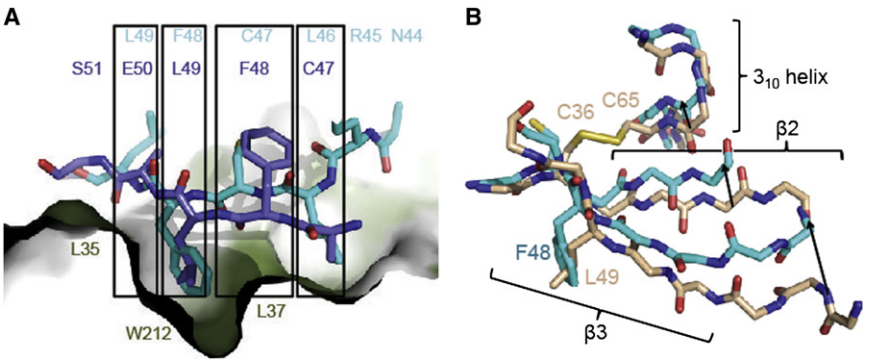

Figure 3. Mobility of Strands β_2 and β_3

(A) Superposition of β_3 of RYR2A Δexon3 chain A (dark blue) and chain B (light blue), indicating the shift in amino acid register. The surface represents the rest of the RYR2A Δexon3. An alternative view is presented in Figure S4.

(B) Superposition of the main chains of β_2, β_3, and the 3_{10} helix of wild-type RYR2A (pink) and RYR2A Δexon3 chain B. RYR2A Δexon3 chain A follows the main chain of the wild-type RYR2A very well and is not shown for clarity. Arrows indicate the relative shifts of the main chains upon deletion of exon 3.

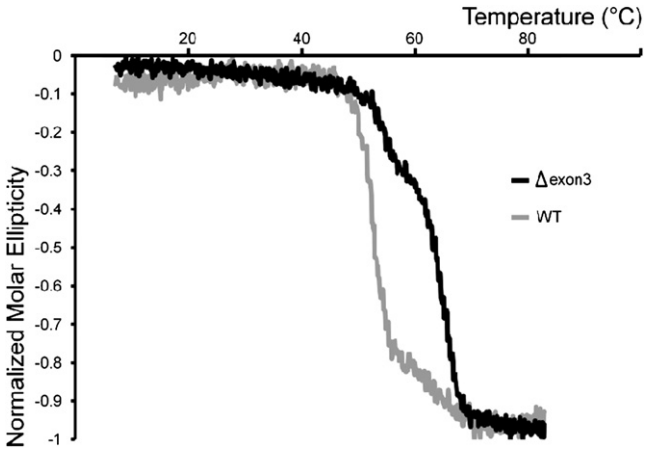

Figure 4. Thermal Unfolding

Thermal melting curves for wild-type (WT) RYR2A (gray) and RYR2A Δexon3 (black) using CD at 217 nm. The data are normalized. Increasing temperature leads to a more negative molar ellipticity.

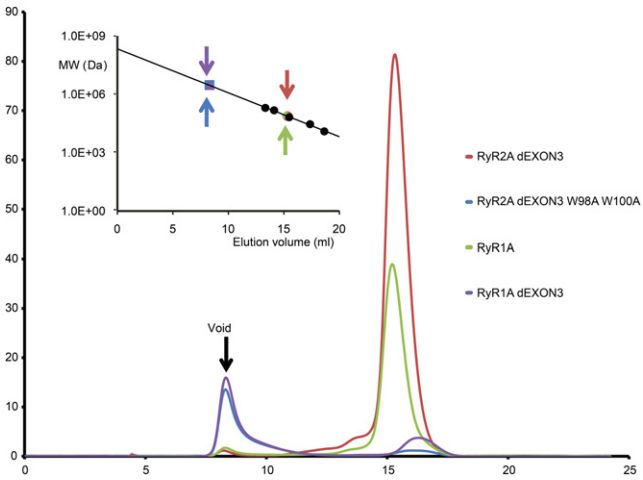

Figure 5. Size Exclusion Chromatography

Gel filtration (Superdex 200) chromatograms for various N-terminal domain constructs fused to MBP. The curve for RYR1A Δexon 3 has been scaled up slightly for clarity. The arrow indicates the void volume. Inset: plot of molecular weight (logarithmic scale) versus elution volume. Black dots indicate molecular weight standards, and the line corresponds to a linear fit of log(MW) versus elution volume. Arrows indicate the four samples. Both RYR1A Δexon3 and RYR2A Δexon3/W98A/F100A are mainly present near the void volume, indicating large aggregation. Expected / observed molecular weights: RYR2A Δexon3 (65.1/74.7 kDa), RYR2A Δexon3 WF-AA (64.9/2890 kDa), RYR1A(67.2/78.9 kDa), RYR1A Δexon3 (63.6/2850 kDa).

the exon 3 deletion, as this removes C65, a cysteine residue involved in a labile disulfide bridge with C36 (Lobo and Van Petegem, 2009). The C36 side chain now points in a different direction (Figure 3B). Because C36 is incapable of forming a disulfide bridge with the deleted C65, restraints on the main chain of β_2 are removed, which translates to increased mobility of the neighboring strand β_3. The overall structural plasticity in RYR2A likely facilitates the incorporation of an entirely different segment into the fold. The conformational changes are shown in Movie S1.

Thermal Melting Analysis of the RYR2 Δexon3 Mutation

We previously found the RYR2A Δexon3 variant to be still soluble and to be thermally more stable than wild-type RYR2A (Lobo and Van Petegem, 2009). The used fluorophore (Sypro Orange) reports on the hydrophobicity of the environment, and hence the availability of hydrophobic residues as the protein unfolds. In order to see whether this effect extends to secondary structure unfolding, and to increase the resolution of the unfolding transitions, we revisited this phenomenon using circular dichroism (CD). Figure 4 shows thermal melting curves using the CD signal at 217 nm for RYR2A and RYR2A Δexon3. The exon 3 deletion shows two distinct transitions, with midpoints around 55°C and 66°C, which correspond well with the previously reported values using thermofluor (Lobo and Van Petegem, 2009). Whereas earlier experiments had shown a single transition for wild-type RYR2A, the CD melting uncovers a smaller transition at higher temperature as well. The main RYR2A transition has a midpoint near 52°C, but the midpoint of the smaller transition could not be obtained in a reliable manner with either a Boltzmann fit or a first derivative plot. It therefore seems that the wild-type RYR2A domain unfolds in two steps, and that the exon 3 deletion causes a significant stabilization of one of the individual folding units.

The Importance of RYR2 Residues W98 and F100 in Rescue of Δexon3

If the RYR2 α_1-β_5 loop is responsible for replacing exon 3, then the removal of key residues in this segment should cause misfolding of the protein. Because the structure suggests that W98 and F100 seemed to make the most extensive interactions, binding into deep hydrophobic pockets, we prepared the double mutation W98A/F100A in the RYR2A Δexon3 background. The protein was expressed as a fusion protein with maltose binding protein (MBP) at its N terminus. An analytical gel filtration chromatogram shows that the fusion protein elutes in the void volume of the column (Figure 5), indicating heavy aggregation likely due to misfolding.

The rescue loop is unique to RYR2 (Lobo and Van Petegem, 2009). An extensive sequence comparison shows that it is only present in RYR2 from mammals and birds, but not in any RyR from other vertebrates or in invertebrates. In the sequences that do contain the insert, the residues are highly conserved (Figure 6).

Because RYR1 misses all of the residues that replace exon 3, a deletion of exon 3 should not be tolerated in this isoform. We prepared a Δexon3 variant of RYR1A (residues 1–205), and gel filtration chromatography of the fusion protein also indicated strong aggregation, likely due to misfolding (Figure 5). An exon 3 deletion in full-length RYR1 is therefore highly likely to have a more drastic effect than in RYR2.

The Exon 3 Deletion Affects Interfaces with Other RyR Domains

Although the lost β strand is rescued, the RYR2 exon 3 deletion still causes a very severe phenotype (Bhuiyan et al., 2007). Despite conservation of the β trefoil core, the α helix is not replaced, and the loop preceding the 3_{10} helix is shortened by 4 residues. In addition, the identities of residues in the rescue

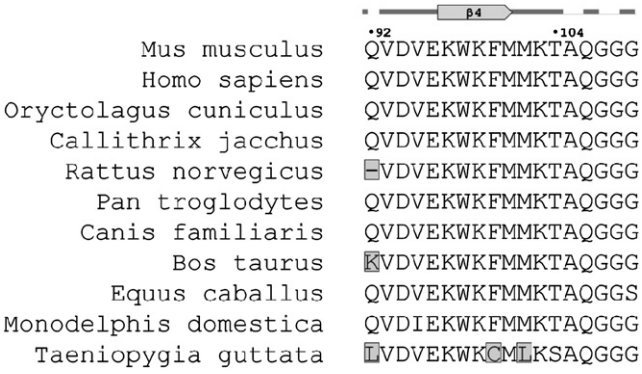

Figure 6. Sequence Alignment of the Rescue Segment in RYR2 from Various Species

The segment is only found in RYR2 from mammals and birds. With the exception of one species (*Taeniopygia guttata*), all residues are highly conserved. A sequence alignment of wild-type and mutant segments in shown in Figure S2.

segment are completely different from the corresponding exon 3 residues.

A crystal structure of the first three domains of RYR1 was recently solved (Tung et al., 2010). The three domains (A,B,C) interact with each other and because of the high sequence conservation in this region, the overall structure and domain-domain interfaces are likely similar in RYR2. We therefore superposed the RYR2A domain onto the RYR1ABC structure (Figure 7A). Residues belonging to exon 3, in particular the 3_{10} helix and preceding loop, are involved in contacts with both domain B and C. The α helix is involved in an interface with electron dense columns extending toward the transmembrane segment (Figures 7B and 7C; Movie S2). Deletion of the helix would therefore completely disrupt this interface, thus being responsible for a very severe disease phenotype.

DISCUSSION

Distinct mutations in RYR2 are known to result in CPVT. According to the current model, the combined effect of catecholamines and disease mutations causes premature or prolonged leak of Ca^{2+} into the cytoplasm, inadvertently activating the Na^+/Ca^{2+} exchanger. The latter is responsible for the efflux of one Ca^{2+} ion in return for the influx of three Na^+ ions, an electrogenic event that can result in delayed after depolarizations (Fozzard, 1992; Marban et al., 1986). A number of CPVT causing mutations in RYR2 have been studied at the molecular level, confirming a gain of function that is compatible with unsolicited Ca^{2+} leak (George et al., 2003; Jiang et al., 2002, 2004, 2005; Koop et al., 2008; MacLennan and Chen, 2009). Loss-of-function mutations cause a very different phenotype, known as catecholaminergic idiopathic ventricular fibrillation (Jiang et al., 2007). Almost all known RYR2 disease mutations are single amino acid substitutions, primarily focused in three "hot spots" located in the N-terminal region, a central domain, and the presumed transmembrane region. Some mutations have been found outside of these regions, and the apparent presence of hot spots could be due to a sequencing bias (Betzenhauser and Marks, 2010; Robinson et al., 2006). A very severe form of CPVT is caused not by a simple amino acid substitution, but by the deletion of the entire third exon in the N-terminal domain of RYR2. Because this 35 amino acid exon forms an integral part of the domain, it is surprising that its deletion does not cause general misfolding and aggregation, an effect that would preclude a gain of function typically associated with CPVT.

We solved a crystal structure of the Δexon3 variant of the RYR2 N-terminal domain at 2.3 Å resolution. An unusual rearrangement is responsible for the structural rescue of the domain: a 12 amino acid stretch in a flexible loop salvages the β trefoil core by substituting both a 3_{10} helix and β strand lost by the deletion. The contacts with the rescue segment are more extensive than with the original β strand, explaining the improved thermal stability of the protein. The rescue is accompanied by shifts in the main chain of two other β strands, one of which undergoes a 1 residue translation in the sequence register. The latter shifts are not strictly required, as they are only observed in one of the two molecules in the asymmetric unit. Overall, these conformational changes highlight the unusual structural plasticity of the RYR2 N-terminal domain.

The exon 3 residues are involved in two interfaces, including interactions with the neighboring domain B, and with electron dense columns that connect the N-terminal domain with the transmembrane region. Single point mutations in both regions have already been shown to cause disease. In particular, mutations in strand β_4 and the preceding 3_{10} helix are known to cause CPVT in RYR2 (L62F) (Medeiros-Domingo et al., 2009) and malignant hyperthermia in RYR1 (D60N, S71Y). These underline the importance of this domain-domain interaction, and a replacement of the interface with a completely dissimilar sequence is therefore likely to destabilize this interaction drastically. In addition, the deleted α helix seems to play a prime role in normal RyR function, as individual point mutations on α_1 (A77V, M81L) are known to cause CPVT (d'Amati et al., 2005; Medeiros-Domingo et al., 2009). The A77V mutation is known to cause only local changes to the RYR2A surface, suggesting this forms an important interaction site with neighboring RYR2 domains (Lobo and Van Petegem, 2009). The recent crystal structure of the N-terminal hot spot has allowed an unambiguous placement of this segment into the available cryo-EM maps of RYR1 (Tung et al., 2010). The hot spot is located in the cytoplasmic area, forming a continuous 240 kDa ring around the 4-fold axis.

Cryo-EM studies comparing RYR1 in the open and closed state have shown that the N-terminal hot spot is involved in extensive conformational changes (Samso et al., 2009; Tung et al., 2010). Based on these observations, we postulate the following working hypothesis. Normal gating of the channel includes an allosteric coupling between the transmembrane region and the N-terminal hot spot. The latter acts as a brake on channel opening. Domain A forms a link through an interface involving the α-helical segment and electron dense columns reaching toward the transmembrane segment (Figures 7B–7D). In addition, other links may exist through coupling of domain A with domains B, C, and other RyR domains. Movement in the pore region therefore necessitates a relative motion of domain A, a process that requires free energy through the disruption of several weak interactions. This energy is normally obtained from bound ligands and proteins in a regulated fashion.

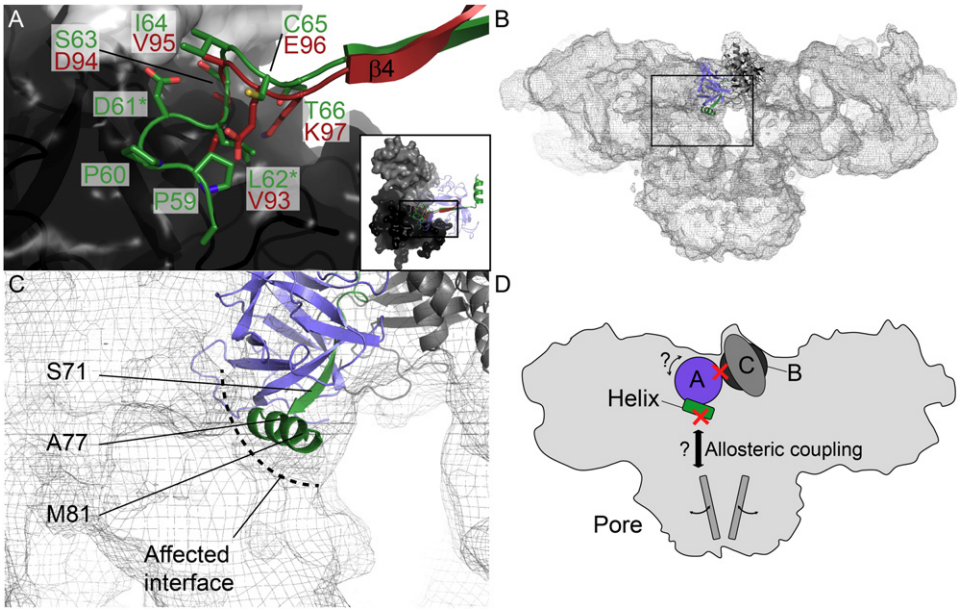

Figure 7. The Exon 3 Deletion Affects Two Interfaces within Full-Length RYR2

(A) Hybrid model consisting of RYR2A exon 3 (green) or the rescue segment (red) and RYR1BC (gray surface) derived from the RYR1ABC structure. Although details within the A-B interface likely differ between RYR1 and RYR2, the high sequence similarity suggests that exon 3 is also involved in contacts with domain B in RYR2.

(B and C) Position of RYR2A and exon 3 within the RyR cryo-EM map. Only one monomer is shown for clarity. The helix is part of an interface with a RyR domain that extends toward the transmembrane region.

(D) Model for the effect of the exon 3 deletion on channel gating. Movement within the transmembrane region is allosterically coupled to the N-terminal domains, involving motions of RYR2A relative to neighboring domains. Disruption of two interfaces reduces the energetic cost to move RYR2A, resulting in facilitated pore opening.

Weakening the contacts of domain A with at least three neighboring domains thus allows for conformational changes with a lower energetic penalty. This then allows for facilitated opening of the pore, resulting in inadvertent Ca^{2+} release under conditions that are normally insufficient to open the pore. The disease phenotype is only revealed upon adrenergic stimulation, involving a role for PKA. The PKA phosphorylation site is not in the N-terminal region, and is likely at the outer surface of the RyR (Jones et al., 2008). It therefore seems that the transmembrane region is under the control of multiple allosteric sites, and that the combined effect of disturbing multiple brakes (e.g., through disease mutation and PKA phosphorylation) leads to channel opening.

The natural question arises about the identity of the regions contacting domain A. Several groups have suggested that the N-terminal hot spot may interact directly with the central disease hot spot (Ikemoto and Yamamoto, 2002; Liu et al., 2010; Tateishi et al., 2009). Based on the distribution of mutations in the N-terminal hot spot however, it is likely that the second hot spot cannot cover all observed interfaces between the domains ABC and other RyR domains (Tung et al., 2010). The identity of the electron dense columns therefore remains to be found. In addition, since the RYR2A α helix is also involved in a lateral interface (Tung et al., 2010), it cannot be excluded that coupling to the pore occurs through other contact regions as well.

The rescue segment is unique to the RYR2 isoform. We therefore predict that a similar mutation in the skeletal muscle isoform, RYR1, may have more drastic consequences for the overall RYR1 structure. In agreement with this, the Δexon3 variant of the RYR1 N-terminal domain heavily aggregates. Comparing the RYR2 sequences of various species reveals that the rescue segment only evolved late, as it is only observed in RyRs from birds and mammals. Within these groups, the segment is highly conserved, suggesting a functional role.

The number of possible sequences with a 12 amino acid stretch is $\sim 4 \times 10^{15}$. Even with some degree of structural plasticity, it is implausible that the RYR2 α_1-β_5 loop is able to insert itself in a β sheet by mere chance. Instead, evolutionary pressure seems to have evolved a unique segment that can specifically form part of the β trefoil domain. Two different scenarios could be considered. In the first, the two segments are in direct competition for the same site in the β trefoil core. Because the rescue segment appears to have a higher thermal stability, one could argue for this segment to be favored. However, the N-terminal end of the rescue segment immediately follows the α helix in wild-type RYR2A, placing it ~37 Å away from its observed position in RYR2A Δexon3. In order for this stretch to be part of the β sheet in wild-type RYR2, the α helix cannot be at its observed location in the wild-type RYR2A structure, which would add an energetic penalty. Given the constant position of the helix in all solved wild-type and mutant structures of the first domain (Amador et al., 2009; Lobo and Van Petegem, 2009; Tung et al., 2010), the rescue segment is only likely to compete if another domain or protein is interacting with the helix. Four different structures are available for "full-length" RYR2A: two point mutants (A77V, V186M), and two molecules in the asymmetric unit of the wild-type crystal structure

(Lobo and Van Petegem, 2009). In all cases, the rescue segment is part of a flexible loop, confirming that this is the most favored conformation in the absence of additional stabilizing elements. However, this is only a property intrinsic to the isolated domain A, and in the context of the full-length channel, the melting temperature and preferred conformation may differ.

A second, more attractive, scenario is alternative splicing, whereby a splice variant missing exon 3 has a tissue-specific role. Due to the clear disease phenotype it is unlikely that such a splice variant would be widely expressed in the heart. Many other tissues however are known to express RYR2, including various parts of the central nervous system (Ledbetter et al., 1994). The main effect of such alternative splicing would be to remove the α-helical segment, representing an interesting setup: rather than removing the α helix individually, the splicing would remove several segments and then replace everything but the helix. Although a Δexon3 splice variant has not yet been identified in nondiseased individuals, RYR2 messenger transcripts in pancreatic islets, cerebrum, and cerebellum have been found to miss an important part of the rescue segment, deleting 7 residues that include W98 (Takasawa et al., 2010). These RYR2 variants have no significant difference in ryanodine binding or expression levels, suggesting that the rescue segment only has a functional role when exon 3 has been removed.

Because Ca^{2+} is a very potent intracellular second messenger, fine-tuning the total amount and time of its entry into the cytoplasm is of prime importance. The structure of the RYR2A Δexon3 domain suggests that the ryanodine receptor has evolved an additional means to regulate Ca^{2+} release, by altering the shape of an individual domain. Future work will shed light on the precise functional role of the rescue segment in wild-type channels, and on the mechanistic steps that lead to increased channel opening upon deletion of the RYR2 third exon.

EXPERIMENTAL PROCEDURES

Cloning, Expression, and Purification

A full-length *ryr2* Δexon3 cDNA clone was obtained from the lab of Wayne Chen (University of Calgary). The corresponding N-terminal domain (residues 1–217) was cloned into the pET28HMT vector as described before (Lobo and Van Petegem, 2009). The fusion protein was expressed in *Escherichia coli* Rosetta (DE3) pLacI and selenomethionine labeling was performed using the adjusted autoinduction media (Studier, 2005). Point mutations were generated using the quikchange protocol (Stratagene). The rabbit RYR1 Δexon3 N-terminal domain (residue 1–205) was obtained by separate PCR of two fragments (residues 1–56 and 92–205) which were ligated using a flanking BamHI site and cloned into pET28HMT.

The purification of RYR2A Δexon3 was performed as for WT RYR2A (Lobo and Van Petegem, 2009). For the RYR1A Δexon3 and RYR2A Δexon3/W98A/F100A proteins, cell lysate was loaded on a PorosMC column (Tosoh Biosep), and eluted with buffer A (250 mM KCl + 10 mM HEPES [pH 7.4]) + 300 mM imidazole. The elution was dialyzed against buffer A, applied to an amylose column (New England Biolabs) and eluted with buffer A + 10 mM maltose. Five hundred microliter of the elution was applied to an analytical Superdex200 column (GE Healthcare) in buffer A.

Circular Dichroism

RYR2A and RYR2A ΔExon3 were dialyzed against 10 mM Na_3PO_4 (pH 7.4), 50 mM KCl, and 2 mM β-mercaptoethanol. Concentrations were determined using the calculated extinction coefficient at 280 nm in the presence of 6 M Guanidine (Edelhoch, 1967). Thermal melts were performed using a Jasco J810 CD spectropolarimeter on samples at a concentration of 5 μM. Prior to the temperature scan, CD spectra of the samples and dialysis buffer alone were collected over a spectral window of 190–300 nm at 25°C. The wavelength was then fixed at 217 nm while the temperature was increased from 7°C to 83°C at a rate of 1°C/min. The midpoints of the transitions in the melting curves were obtained by taking the maximum values of the slopes.

Table 1. Data Collection and Refinement Statistics

	RYR2A Δexon3
Data collection	
Space group	C2
Cell dimensions	
a, *b*, *c* (Å)	95.370, 44.204, 76.606
α,β,γ (°)	90.00 90.98 90.00
Resolution (Å)	50.00–2.30 (2.38-2.30)[a]
R_{sym} or R_{merge}	0.065 (0.200)
I / σ(I)	10.8 (2.4)
Completeness (%)	84.5 (32.9)
Redundancy	1.8 (1.3)
Refinement	
Resolution (Å)	38.29–2.30
No. reflections	12,259
R_{work} / R_{free}	0.209/0.250
No. atoms	2380
Protein	2338
Water	42
B-factors	
Protein	50.0
Water	44.6
Rmsds	
Bond lengths (Å)	0.012
Bond angles (°)	1.435
Ramachandran (core/allowed %)	89.6/10.4

[a] Values in parentheses are for highest resolution shell.

Crystallization and Data Collection

Crystals were obtained by hanging drop vapor diffusion at 10%–15% PEG 1000. They were transferred to the same condition supplemented with 25% 2-methyl-2,4-pentanediol and flash-cooled in liquid nitrogen. Data sets were obtained at the Stanford Synchrotron Radiation Lightsource (SSRL) beamline 11-1 and the Canadian Light Source (CLS) beamline 08ID-1, and processed using the HKL2000 package (HKL Research). The best data used to solve and refine the structure were collected at 0.9729 Å.

Structure Solution and Refinement

A model consisting of the structure of wild-type RYR2A (PDB 3IM5) without residues 57–91 was used for molecular replacement by Phaser (McCoy et al., 2007). An anomalous difference map was created to confirm the positions of methionines in the rescue segment. Successive rounds of manual modeling in COOT (Emsley and Cowtan, 2004) and refinement using REFMAC5 (Murshudov et al., 1997), with TLS restraints applied to the individual molecules of the asymmetric unit, led to the final structure. A composite omit map was calculated with Phenix (Adams et al., 2010) to verify the absence of residual model bias. Refinement statistics are available in Table 1.

ACCESSION NUMBERS

Coordinates and structure factors for the RYR2A Δexon3 structures have been deposited in the Protein Data Bank with accession code 3QR5.

SUPPLEMENTAL INFORMATION

Supplemental Information includes four figures and two movies and can be found with this article online at doi:10.1016/j.str.2011.03.016.

ACKNOWLEDGMENTS

We thank Dr. Wayne Chen (U. of Calgary) for the full-length RYR2 Δexon3 clone. Diffraction experiments were performed at the Stanford Synchrotron Radiation Laboratory (Palo Alto, USA) and the Canadian Light Source (Saskatoon, Canada), which is supported by the Natural Sciences and Engineering Research Council of Canada, the National Research Council Canada, the Canadian Institutes of Health Research (CIHR), the Province of Saskatchewan, Western Economic Diversification Canada, and the University of Saskatchewan. F.V.P. is a CIHR new investigator and a Michael Smith Foundation of Health Research (MSFHR) career investigator. This work is funded by the Heart and Stroke Foundation of Canada, the Canadian Foundation for Innovation, and the BC Knowledge Development Fund. We declare no conflict of interest.

Received: December 20, 2010
Revised: February 17, 2011
Accepted: March 22, 2011
Published: June 7, 2011

REFERENCES

Adams, P.D., Afonine, P.V., Bunkoczi, G., Chen, V.B., Davis, I.W., Echols, N., Headd, J.J., Hung, L.W., Kapral, G.J., Grosse-Kunstleve, R.W., et al. (2010). PHENIX: a comprehensive Python-based system for macromolecular structure solution. Acta Crystallogr. D Biol. Crystallogr. *66*, 213–221.

Amador, F.J., Liu, S., Ishiyama, N., Plevin, M.J., Wilson, A., MacLennan, D.H., and Ikura, M. (2009). Crystal structure of type I ryanodine receptor amino-terminal beta-trefoil domain reveals a disease-associated mutation "hot spot" loop. Proc. Natl. Acad. Sci. USA *106*, 11040–11044.

Bers, D.M. (2004). Macromolecular complexes regulating cardiac ryanodine receptor function. J. Mol. Cell. Cardiol. *37*, 417–429.

Betzenhauser, M.J., and Marks, A.R. (2010). Ryanodine receptor channelopathies. Pflugers Arch. *460*, 467–480.

Bhuiyan, Z.A., van den Berg, M.P., van Tintelen, J.P., Bink-Boelkens, M.T., Wiesfeld, A.C., Alders, M., Postma, A.V., van Langen, I., Mannens, M.M., and Wilde, A.A. (2007). Expanding spectrum of human RYR2-related disease: new electrocardiographic, structural, and genetic features. Circulation *116*, 1569–1576.

Cabello, A., and Ricoy-Campo, J.R. (2003). [Congenital myopathies]. Rev. Neurol. *37*, 779–786.

d'Amati, G., Bagattin, A., Bauce, B., Rampazzo, A., Autore, C., Basso, C., King, K., Romeo, M.D., Gallo, P., Thiene, G., et al. (2005). Juvenile sudden death in a family with polymorphic ventricular arrhythmias caused by a novel RyR2 gene mutation: evidence of specific morphological substrates. Hum. Pathol. *36*, 761–767.

Edelhoch, H. (1967). Spectroscopic determination of tryptophan and tyrosine in proteins. Biochemistry *6*, 1948–1954.

Emsley, P., and Cowtan, K. (2004). Coot: model-building tools for molecular graphics. Acta Crystallogr. D Biol. Crystallogr. *60*, 2126–2132.

Fozzard, H.A. (1992). Afterdepolarizations and triggered activity. Basic Res. Cardiol. *87* (*Suppl 2*), 105–113.

George, C.H., Higgs, G.V., and Lai, F.A. (2003). Ryanodine receptor mutations associated with stress-induced ventricular tachycardia mediate increased calcium release in stimulated cardiomyocytes. Circ. Res. *93*, 531–540.

George, C.H., Jundi, H., Thomas, N.L., Fry, D.L., and Lai, F.A. (2007). Ryanodine receptors and ventricular arrhythmias: emerging trends in mutations, mechanisms and therapies. J. Mol. Cell. Cardiol. *42*, 34–50.

Giannini, G., Conti, A., Mammarella, S., Scrobogna, M., and Sorrentino, V. (1995). The ryanodine receptor/calcium channel genes are widely and differentially expressed in murine brain and peripheral tissues. J. Cell Biol. *128*, 893–904.

Hakamata, Y., Nakai, J., Takeshima, H., and Imoto, K. (1992). Primary structure and distribution of a novel ryanodine receptor/calcium release channel from rabbit brain. FEBS Lett. *312*, 229–235.

Ikemoto, N., and Yamamoto, T. (2002). Regulation of calcium release by interdomain interaction within ryanodine receptors. Front. Biosci. *7*, d671–d683.

Jiang, D., Xiao, B., Zhang, L., and Chen, S.R. (2002). Enhanced basal activity of a cardiac Ca2+ release channel (ryanodine receptor) mutant associated with ventricular tachycardia and sudden death. Circ. Res. *91*, 218–225.

Jiang, D., Xiao, B., Yang, D., Wang, R., Choi, P., Zhang, L., Cheng, H., and Chen, S.R. (2004). RyR2 mutations linked to ventricular tachycardia and sudden death reduce the threshold for store-overload-induced Ca2+ release (SOICR). Proc. Natl. Acad. Sci. USA *101*, 13062–13067.

Jiang, D., Wang, R., Xiao, B., Kong, H., Hunt, D.J., Choi, P., Zhang, L., and Chen, S.R. (2005). Enhanced store overload-induced Ca2+ release and channel sensitivity to luminal Ca2+ activation are common defects of RyR2 mutations linked to ventricular tachycardia and sudden death. Circ. Res. *97*, 1173–1181.

Jiang, D., Chen, W., Wang, R., Zhang, L., and Chen, S.R. (2007). Loss of luminal Ca2+ activation in the cardiac ryanodine receptor is associated with ventricular fibrillation and sudden death. Proc. Natl. Acad. Sci. USA *104*, 18309–18314.

Jiang, D., Chen, W., Xiao, J., Wang, R., Kong, H., Jones, P.P., Zhang, L., Fruen, B., and Chen, S.R. (2008). Reduced threshold for luminal Ca2+ activation of RyR1 underlies a causal mechanism of porcine malignant hyperthermia. J. Biol. Chem. *283*, 20813–20820.

Jones, P.P., Meng, X., Xiao, B., Cai, S., Bolstad, J., Wagenknecht, T., Liu, Z., and Chen, S.R. (2008). Localization of PKA phosphorylation site, Ser(2030), in the three-dimensional structure of cardiac ryanodine receptor. Biochem. J. *410*, 261–270.

Koop, A., Goldmann, P., Chen, S.R., Thieleczek, R., and Varsanyi, M. (2008). ARVC-related mutations in divergent region 3 alter functional properties of the cardiac ryanodine receptor. Biophys. J. *94*, 4668–4677.

Laitinen, P.J., Brown, K.M., Piippo, K., Swan, H., Devaney, J.M., Brahmbhatt, B., Donarum, E.A., Marino, M., Tiso, N., Viitasalo, M., et al. (2001). Mutations of the cardiac ryanodine receptor (RyR2) gene in familial polymorphic ventricular tachycardia. Circulation *103*, 485–490.

Ledbetter, M.W., Preiner, J.K., Louis, C.F., and Mickelson, J.R. (1994). Tissue distribution of ryanodine receptor isoforms and alleles determined by reverse transcription polymerase chain reaction. J. Biol. Chem. *269*, 31544–31551.

Lehnart, S.E., Wehrens, X.H., Reiken, S., Warrier, S., Belevych, A.E., Harvey, R.D., Richter, W., Jin, S.L., Conti, M., and Marks, A.R. (2005). Phosphodiesterase 4D deficiency in the ryanodine-receptor complex promotes heart failure and arrhythmias. Cell *123*, 25–35.

Lehnart, S.E., Mongillo, M., Bellinger, A., Lindegger, N., Chen, B.X., Hsueh, W., Reiken, S., Wronska, A., Drew, L.J., Ward, C.W., et al. (2008). Leaky Ca2+ release channel/ryanodine receptor 2 causes seizures and sudden cardiac death in mice. J. Clin. Invest. *118*, 2230–2245.

Liu, Z., Zhang, J., Sharma, M.R., Li, P., Chen, S.R., and Wagenknecht, T. (2001). Three-dimensional reconstruction of the recombinant type 3 ryanodine receptor and localization of its amino terminus. Proc. Natl. Acad. Sci. USA *98*, 6104–6109.

Liu, Z., Wang, R., Tian, X., Zhong, X., Gangopadhyay, J., Cole, R., Ikemoto, N., Chen, S.R., and Wagenknecht, T. (2010). Dynamic, inter-subunit interactions between the N-terminal and central mutation regions of cardiac ryanodine receptor. J. Cell Sci. *123*, 1775–1784.

Lobo, P.A., and Van Petegem, F. (2009). Crystal structures of the N-terminal domains of cardiac and skeletal muscle ryanodine receptors: insights into disease mutations. Structure *17*, 1505–1514.

Ludtke, S.J., Serysheva, I.I., Hamilton, S.L., and Chiu, W. (2005). The pore structure of the closed RyR1 channel. Structure *13*, 1203–1211.

MacLennan, D.H., and Phillips, M.S. (1992). Malignant hyperthermia. Science *256*, 789–794.

MacLennan, D.H., and Chen, S.R. (2009). Store overload-induced Ca2+ release as a triggering mechanism for CPVT and MH episodes caused by mutations in RYR and CASQ genes. J. Physiol. *587*, 3113–3115.

Marban, E., Robinson, S.W., and Wier, W.G. (1986). Mechanisms of arrhythmogenic delayed and early afterdepolarizations in ferret ventricular muscle. J. Clin. Invest. *78*, 1185–1192.

Marjamaa, A., Laitinen-Forsblom, P., Lahtinen, A.M., Viitasalo, M., Toivonen, L., Kontula, K., and Swan, H. (2009). Search for cardiac calcium cycling gene mutations in familial ventricular arrhythmias resembling catecholaminergic polymorphic ventricular tachycardia. BMC Med. Genet. *10*, 12.

Marx, S.O., Reiken, S., Hisamatsu, Y., Jayaraman, T., Burkhoff, D., Rosemblit, N., and Marks, A.R. (2000). PKA phosphorylation dissociates FKBP12.6 from the calcium release channel (ryanodine receptor): defective regulation in failing hearts. Cell *101*, 365–376.

Maximciuc, A.A., Putkey, J.A., Shamoo, Y., and Mackenzie, K.R. (2006). Complex of calmodulin with a ryanodine receptor target reveals a novel, flexible binding mode. Structure *14*, 1547–1556.

McCoy, A.J., Grosse-Kunstleve, R.W., Adams, P.D., Winn, M.D., Storoni, L.C., and Read, R.J. (2007). Phaser crystallographic software. J. Appl. Crystallgr. *40*, 658–674.

Medeiros-Domingo, A., Bhuiyan, Z.A., Tester, D.J., Hofman, N., Bikker, H., van Tintelen, J.P., Mannens, M.M., Wilde, A.A., and Ackerman, M.J. (2009). The RYR2-encoded ryanodine receptor/calcium release channel in patients diagnosed previously with either catecholaminergic polymorphic ventricular tachycardia or genotype negative, exercise-induced long QT syndrome: a comprehensive open reading frame mutational analysis. J. Am. Coll. Cardiol. *54*, 2065–2074.

Murshudov, G.N., Vagin, A.A., and Dodson, E.J. (1997). Refinement of macromolecular structures by the maximum-likelihood method. Acta Crystallogr. D Biol. Crystallogr. *53*, 240–255.

Priori, S.G., Napolitano, C., Tiso, N., Memmi, M., Vignati, G., Bloise, R., Sorrentino, V., and Danieli, G.A. (2001). Mutations in the cardiac ryanodine receptor gene (hRyR2) underlie catecholaminergic polymorphic ventricular tachycardia. Circulation *103*, 196–200.

Robinson, R., Carpenter, D., Shaw, M.A., Halsall, J., and Hopkins, P. (2006). Mutations in RYR1 in malignant hyperthermia and central core disease. Hum. Mutat. *27*, 977–989.

Samso, M., Wagenknecht, T., and Allen, P.D. (2005). Internal structure and visualization of transmembrane domains of the RyR1 calcium release channel by cryo-EM. Nat. Struct. Mol. Biol. *12*, 539–544.

Samso, M., Feng, W., Pessah, I.N., and Allen, P.D. (2009). Coordinated movement of cytoplasmic and transmembrane domains of RyR1 upon gating. PLoS Biol. *7*, e85.

Sharma, M.R., Penczek, P., Grassucci, R., Xin, H.B., Fleischer, S., and Wagenknecht, T. (1998). Cryoelectron microscopy and image analysis of the cardiac ryanodine receptor. J. Biol. Chem. *273*, 18429–18434.

Shepherd, S., Ellis, F., Halsall, J., Hopkins, P., and Robinson, R. (2004). RYR1 mutations in UK central core disease patients: more than just the C-terminal transmembrane region of the RYR1 gene. J. Med. Genet. *41*, e33.

Studier, F.W. (2005). Protein production by auto-induction in high density shaking cultures. Protein Expr. Purif. *41*, 207–234.

Takasawa, S., Kuroki, M., Nata, K., Noguchi, N., Ikeda, T., Yamauchi, A., Ota, H., Itaya-Hironaka, A., Sakuramoto-Tsuchida, S., Takahashi, I., et al. (2010). A novel ryanodine receptor expressed in pancreatic islets by alternative splicing from type 2 ryanodine receptor gene. Biochem. Biophys. Res. Commun. *397*, 140–145.

Tateishi, H., Yano, M., Mochizuki, M., Suetomi, T., Ono, M., Xu, X., Uchinoumi, H., Okuda, S., Oda, T., Kobayashi, S., et al. (2009). Defective domain-domain interactions within the ryanodine receptor as a critical cause of diastolic Ca2+ leak in failing hearts. Cardiovasc. Res. *81*, 536–545.

Thomas, N.L., George, C.H., Williams, A.J., and Lai, F.A. (2007). Ryanodine receptor mutations in arrhythmias: advances in understanding the mechanisms of channel dysfunction. Biochem. Soc. Trans. *35*, 946–951.

Tung, C.C., Lobo, P.A., Kimlicka, L., and Van Petegem, F. (2010). The amino-terminal disease hotspot of ryanodine receptors forms a cytoplasmic vestibule. Nature *468*, 585–588.

Wang, R., Chen, W., Cai, S., Zhang, J., Bolstad, J., Wagenknecht, T., Liu, Z., and Chen, S.R. (2007). Localization of an NH(2)-terminal disease-causing mutation hot spot to the "clamp" region in the three-dimensional structure of the cardiac ryanodine receptor. J. Biol. Chem. *282*, 17785–17793.

Wright, N.T., Prosser, B.L., Varney, K.M., Zimmer, D.B., Schneider, M.F., and Weber, D.J. (2008). S100A1 and calmodulin compete for the same binding site on ryanodine receptor. J. Biol. Chem. *283*, 26676–26683.

Zalk, R., Lehnart, S.E., and Marks, A.R. (2007). Modulation of the ryanodine receptor and intracellular calcium. Annu. Rev. Biochem. *76*, 367–385.

